# Composition- and Band-Gap-Tunable Synthesis of Wurtzite-Derived Cu$_2$ZnSn(S$_{1-x}$Se$_x$)$_4$ Nanocrystals: Theoretical and Experimental Insights

Feng-Jia Fan,[†] Liang Wu,[†] Ming Gong,[‡] Guangyao Liu,[§] Yi-Xiu Wang,[†] Shu-Hong Yu,[†,*] Shiyou Chen,[⊥,*] Lin-Wang Wang,[∥] and Xin-Gao Gong[#]

[†]Division of Nanomaterials & Chemistry, Hefei National Laboratory for Physical Sciences at Microscale, Department of Chemistry, University of Science and Technology of China, Hefei 230026, People's Republic of China, [‡]Engineering and Materials Science Experiment Center, University of Science and Technology of China, Hefei 230026, People's Republic of China, [§]Beijing National Laboratory for Condensed Matter Physics, Institute of Physics, Chinese Academy of Sciences, Beijing 100190, People's Republic of China, [⊥]Key Laboratory of Polar Materials and Devices (MOE), East China Normal University, Shanghai 200241, People's Republic of China, [∥]Materials Sciences Division, Lawrence Berkeley National Laboratory, One Cyclotron Road, Mail Stop 66, Berkeley, California 94720, United States, and [#]Key Laboratory for Computational Physical Sciences (MOE) and Department of Physics, Fudan University, Shanghai 200433, People's Republic of China

ABSTRACT The wurtzite-derived Cu$_2$ZnSn(S$_{1-x}$Se$_x$)$_4$ alloys are studied for the first time through combining theoretical calculations and experimental characterizations. *Ab initio* calculations predict that wurtzite-derived Cu$_2$ZnSnS$_4$ and Cu$_2$ZnSnSe$_4$ are highly miscible, and the band gaps of the mixed-anion alloys can be linearly tuned from 1.0 to 1.5 eV through changing the composition parameter x from 0 to 1. A synthetic procedure for the wurtzite-derived Cu$_2$ZnSn(S$_{1-x}$Se$_x$)$_4$ alloy nanocrystals with tunable compositions has been developed. A linear tunable band-gap range of 0.5 eV is observed in the synthesized alloy nanocrystals, which shows good agreement with the *ab initio* calculations.
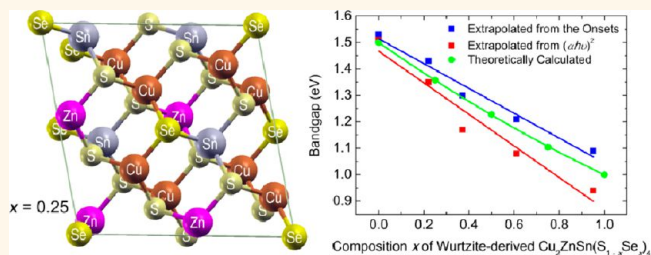
KEYWORDS: wurtzite · Cu$_2$ZnSnS$_4$ · Cu$_2$ZnSnSe$_4$ · alloy · Cu$_2$ZnSn(S$_{1-x}$Se$_x$)$_4$ · miscibility · band gap · nanocrystal

Cu$_2$ZnSnS$_4$ (CZTS), Cu$_2$ZnSnSe$_4$ (CZTSe), and their alloys Cu$_2$ZnSn(S$_{1-x}$Se$_x$)$_4$ (CZTSSe) are ideal substitutes for the currently commercialized solar cell absorber Cu(In$_{1-x}$Ga$_x$)Se$_2$ (CIGSe) semiconductors, because they consist of earth-abundant elements Zn and Sn rather than scarce elements In and Ga, as well as possess strong light absorption and suitable band gaps.[1−3] Recently, an electric efficiency around 10% has been achieved in hydrazine-processed CZTSSe thin-film solar cells,[4,5] demonstrating a promising future.

Printing colloidal "nanocrystal ink" is a novel method to prepare solar cell absorber layers, and the fabricated devices would result in reduced costs.[6−13] Three recent works have demonstrated that this approach can be applied to fabricate CZTSSe, Cu$_2$Zn(Ge$_{1-x}$Sn$_x$)-(S$_{1-y}$Se$_y$)$_4$, and Cu(In$_{1-x}$Ga$_x$)(S$_{1-y}$Se$_y$)$_2$ thin-film solar cells, yielding reasonably high efficiencies

of 7.2%, 8.4%, and 12%, respectively.[14−16] These results encourage the further development of the colloidal "nanocrystal inks" synthesis.[17−21] One interesting discovery about "nanocrystal ink" is that although the wurtzite-derived phases (derived from the wurtzite ZnS or ZnSe structure) of ternary and quaternary chalcogenides, *e.g.*, CuInS$_2$ (CIS),[22] CuInSe$_2$ (CISe),[23] Cu$_2$SnSe$_3$ (CTSe),[24] CZTS,[25] and CZTSe,[26] have never been observed in thin-film samples due to their energetic metastability, they can be prepared in nanocrystals given proper kinetic controls.[22−26] Considering their special structural, surface, and interface properties, which are at variance with those of the ground-state zincblende-derived phases, these wurtzite-derived phases provide new chances to tune their properties and optimize the solar cell performance proceeding from the "nanocrystal ink".

For compound semiconductors, one important way to tune their properties is to form mixed-anion alloys. For example, thanks to the more flexible material properties, the solar cells based on the CZTSSe alloys have achieved higher efficiency than the pure CZTS and CZTSe solar cells.[4,5] It should be noticed that the syntheses of CZTSSe alloys with different compositions have been reported only with the ground zincblende-derived structure, in both thin-film and nanocrystal samples;[20,27−32] however, whether the wurtzite-derived alloys can be synthesized is still an open question. This is important for their applications as solar cell absorbers while challenging because of the two-fold energetic metastability; that is, the CZTSSe alloys are metastable relative to the phase separation into pure CZTS and CZTSe, and the wurtzite-derived CZTSSe are metastable relative to the zincblende-derived CZTSSe. For most of the semiconductor alloys, such as $In_{1−x}Ga_xN$,[33] $GaN_{1−x}As_x$,[34] and $ZnO_{1−x}Se_x$,[35] whether the compositionally homogeneous and tunable samples can be synthesized under a certain temperature depends on the specific miscibility of the mixed elements. Due to the limited study both experimentally and theoretically, these issues are not clear, i.e., whether the mixed-anion CZTSSe alloys in the wurtzite-derived structure have a good miscibility; how their band gaps and optical properties depend on the composition x; and how they differ from the corresponding zincblende-derived alloys.

In this article, we answer these questions and demonstrate that composition- and band-gap-tunable wurtzite-derived CZTSSe alloys are achievable. We first introduce the prediction from the theoretical calculations, then demonstrate the first synthesis and characterizations of wurtzite-derived CZTSSe alloy nanocrystals.

RESULTS AND DISCUSSION

Miscibility of Wurtzite-Derived CZTS and CZTSe. As reported previously, both CZTS and CZTSe crystallize in the zincblende-derived kesterite structure (Figure 1a) at their ground states,[36,37] in which Cu, Zn, and Sn cations occupy one face-centered-cubic (fcc) sublattice of the zincblende structure and the S (or Se) anions occupy the other sublattice. The wurtzite-derived structures are metastable, in which the Cu, Zn, and Sn cations occupy one hexagonal-close-packed (HCP) sublattice of the wurtzite structure and the anions occupy the other sublattice (Figure 1b and Supporting Information Table S1). Among all the wurtzite-derived structures, the wurtzite−kesterite structure shown in Figure 1b has the lowest total energy and can be related to the kesterite structure through a structural rotation, as discussed previously.[37] The wurtzite-derived CZTSSe alloys mean that the isovalent S and Se are mixed on the anion hcp sublattice, and their occupations are usually disordered, like many isovalent alloys, such as $In_{1−x}Ga_xN$[33] and $GaAs_{1−x}P_x$.[38] One key

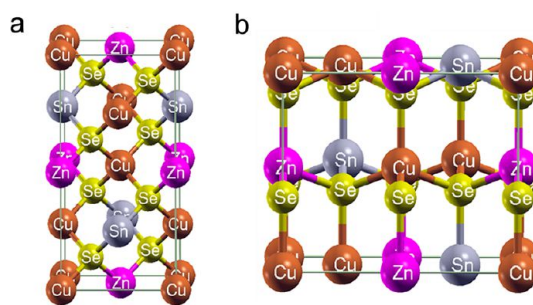
Figure 1. Unit cells of kesterite (a) and wurtzite−kesterite (b) CZTSe. The cations and anions of CZTS and CZTSSe have the same atomic positions as CZTSe, but Se anions are totally or partially substituted by S anions.
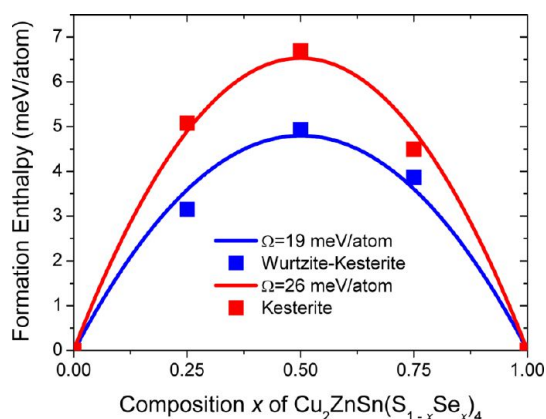

Figure 2. Calculated formation enthalpies of CZTSSe with different composition x (x = 0, 0.25, 0.5, 0.75, and 1) in the wurtzite-derived wurtzite−kesterite and zincblende-derived kesterite structures. The lines show the fitting according to eq 2, with the interaction parameters labeled.

issue in the theoretical simulation of the disordered semiconductor alloys is how to describe the randomness of the isovalent elements using a supercell with finite size. In the present study, the well-established special-quasirandom structures (SQS[39,40]) are used, in which the mixed-anion sites are occupied in a way that the structural correlation functions are close to the exact values of the random alloys, so the calculated formation energy and the band gaps are also close to those of the random alloys. The SQS model with the composition x = 0, 0.25 (equivalent to 0.75), and 0.50 can be plotted (see Supporting Information Figure S1), with the atomic coordinates listed in Table S2.

Figure 2 shows our calculated formation enthalpies of the wurtzite-derived and zincblende-derived (calculation details are given in a previous work[27]) CZTSSe alloys. The formation enthalpies of the alloys are defined as

$$\Delta H_f(x) = E(x) − (1 − x)E(0) − xE(1) \quad (1)$$

where $E(x)$ is the total energy of the CZTSSe alloy at the composition parameter x as calculated using the SQS supercell, and $E(0)$ and $E(1)$ are the total energies of pure CZTS and CZTSe, respectively. The formation

enthalpy $\Delta H_f(x)$ describes the energy cost for mixing S and Se anions in a certain lattice, so $E(0)$ and $E(1)$ of the wurtzite-derived CZTS and CZTSe are used for calculating $\Delta H_f(x)$ of the wurtzite-derived alloys ($E(0)$ and $E(1)$ of the zincblende-derived CZTS and CZTSe for the zincblende-derived alloys). It is obvious that both alloys have an upward bowing in their $\Delta H_f(x)$ dependence on the composition parameter x, which indicates they prefer decoherent phase separation into CZTS and CZTSe at zero temperature. Comparing the two lines, we can find that the formation enthalpies $\Delta H_f(x)$ of wurtzite-derived alloys are always lower than those of zincblende-derived ones at the same composition, which indicates that the S and Se anions can be more easily mixed in the HCP sublattice of the wurtzite-derived structure than in the fcc sublattice of the zincblende-derived structure.

To estimate the miscibility temperature, the calculated formation enthalpies $\Delta H_f(x)$ in Figure 2 are fitted to the following formula:

$$\Delta H_f(x) = \Omega x(1 - x) \qquad (2)$$

where Ω is the alloy interaction parameter,[33] and the fitted values are 19 and 26 meV/atom (38 and 52 meV/mixed-atom) for the wurtzite-derived and zincblende-derived alloys, respectively. In order to mix the S and Se anions, the above positive formation enthalpy has to be overcome by the configuration entropy under a certain temperature, which is $kT[x \ln x + (1 - x)\ln x]$ according to the standard solid solution model. This gives the miscibility temperatures of 220 and 300 K for wurtzite-derived and zincblende-derived CZTSSe alloys, respectively. Both temperatures are below the typical growth temperatures, and thus a good miscibility is expected in the CZTSSe alloys, whether in wurtzite-derived or zincblende-derived structures. This distinguishes CZTSSe alloys from the currently commercialized solar cell materials $Cu(In_xGa_{1-x})Se_2$ (CIGS) alloys, in which the high Ω parameter (a calculated value of 176 meV/mixed-atom[41]) and high miscibility temperature (around 1000 K) make the phase separation and In/Ga inhomogeneity serious in the synthesized samples,[42] especially when Ga composition is high, limiting the solar cell performance. For CZTSSe alloys, component-uniform samples with variable compositions can be synthesized, so the limitation is much weaker, which is an important advantage relative to CIGS.

Theoretical Band-Gap Dependence on Compositions of the Wurtzite-Derived CZTSSe Alloys. Since the composition of CZTSSe alloys can be tuned with a good miscibility, now we will look at how the composition influences the band gap. The band gaps of the thin-film CZTS and CZTSe in the kesterite structure are nowadays clear; they are about 1.5 and 1.0 eV for the stoichiometric samples, respectively.[1,45,46] However, there are still debates about the band gaps of the nanocrystal samples,

TABLE 1. Reported Band Gaps of Zincblende- or Wurtzite-Derived CZTS, CZTSe, and CZTSSe Alloy Nanocrystals

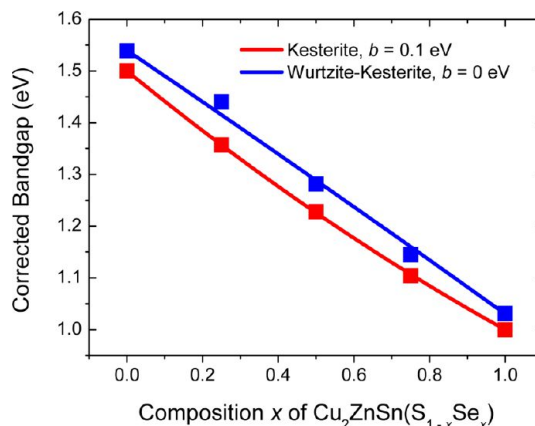| compound	crystal structure	band gap (eV)
CZTS	zincblende derivative	1.3,[13] 1.5,[11,12] 1.5[17]
CZTSe	zincblende derivative	1.4−1.5,[43] 1.3,[17] 1.52[44]
CZTSSe	zincblende derivative	1.47−1.54,[20] 1.28−1.50[28]
CZTS	wurtzite derivative	1.4,[25] 1.43[18]
CZTSe	wurtzite derivative	1.46[26]

Figure 3. Band-gap dependence of the wurtzite-derived (blue) and zincblende-derived (red) CZTSSe alloys on the composition x. The filled squares are the calculated values, and the lines show the change according to the fitted bowing parameter b. Here the GGA calculated band gaps are corrected through adding an error, which changes linearly with x from the calculated error of the CZTSe (1.30 eV) to that of CZTS (1.41 eV).

of which the reported values are listed in Table 1. It seems that the band gap of CZTSe nanocrsytals has been overestimated; for example, the band gap of the zincblende-derived CZTSe was reported to be 1.47 eV[20] (see Table 1), even higher than that of the wurtzite-derived CZTS (1.4 eV from a different paper).[25] Although a band-gap-tunable range from 1.0 to 1.5 eV is expected according to the values of the zincblende-derived thin-film samples, the achievable band-gap range for the wurtzite-derived alloys is still a question.

Figure 3 shows the calculated band gaps for wurtzite-derived (blue) CZTSSe alloys with different compositions, and the values for the zincblende-derived (red) alloys are also plotted to show the difference between the two phases. It is obvious that the band gaps of both wurtzite-derived and zincblende-derived CZTSSe alloys depend almost linearly on the composition x, so the band-gap bowing parameters (labeled in Figure 3) are both small. The band gaps of the wurtzite-derived alloys are always higher than those of the zincblende-derived ones with the same composition x, despite the fact that their differences are always small, less than 0.1 eV. The relatively larger band gaps of the wurtzite-derived structures have been understood for CZTS and CZTSe according to the symmetry of the valence band maximum (VBM) and conduction band

minimum (CBM) states,[37] and the same mechanism also works for CZTSSe alloys. It should be noted that the disorder between Cu and Zn cations is highly possible in the CZTS and CZTSe semiconductors due to the very low energy cost to exchange them.[36] Our calculations have shown that Cu/Zn partial disorder is also possible in the wurtzite-derived CZTSSe alloys, and the specific cation ordering may depend on the growth processes. However, since the partial disorder is universal in CZTSSe with different compositions, its influence on the band gaps (decrease by less than 0.1 eV) is also universal, and thus the relative band gap change is not affected. Thus, although the structural diversity (wurtzite-derived or zincblende-derived, Cu/Zn partially disordered or not) may influence the band gaps, the influence should be in a perturbative and uniform way. A continuous and linear band-gap tuning from about 1.0 to 1.5 eV should be possible through the composition control.

Synthesis and Characterization of Wurtzite-Derived CZTS and CZTSSe Nanocrsytals. To verify the predicted dependence of band gaps on composition parameter x, we developed a high-temperature solvothermal procedure to prepare wurtzite-derived CZTSSe alloy nanocrystals. Various amounts of CuI, $Zn(CH_3COO)_2 \cdot 2H_2O$, and $SnCl_2 \cdot 2H_2O$ listed in Table S3 were used as the cation sources. Since the Zn source shows lower reactivity than the Cu and Sn sources,[47] the reagents contain more Zn salt than the stoichiometric amount for the expected cation ratios. To get metastable wurtzite-derived CZTS and CZTSSe alloy nanocrystals, 1-dodecanethiol and diphenyl diselenide, which have been proven to provide proper kinetic controls to get metastable nanocrystals,[22,23] were added as sulfur and selenium sources, respectively. Sulfur and selenium powders were absent in our synthesis, because reactions yield zincblende-derived products when they are involved.[20] It should be noted that we balanced the reactivities of sulfur and selenium sources through adjusting the molar ratios of 1-dodecanethiol/diphenyl diselenide, and pure CZTS and heavily sulfur-doped CZTSe nanocrystals were prepared through keeping the amount of 1-dodecanethiol constant (600 μL) while varying the amount of diphenyl diselenide from 0 to 0.28 mmol. Actually, 600 μL of 1-dodecanethiol contains about 2.5 mmol of sulfur atoms, which are much more than the stoichiometric values even for the reaction producing pure CZTS nanocrsytals (0.56 mmol), indicating that 1-dodecanethiol is not exhausted after reactions. The remaining 1-dodecanethiol acts as an efficient capping surfactant to ensure the dispersibility of the synthesized nanocrystals. We tried to synthesize pure wurtzite-derived CZTSe without the presence of 1-dodecanethiol; however, the synthesized nanocrystals were hard to disperse in hexane. When 80 μL of 1-dodecanethiol is added into the reaction mixture, the obtained nanocrystals show largely improved

TABLE 2. Cation Ratios and Composition x of the Synthesized Wurtzite-Derived CZTS and CZTSSe Alloy Nanocrystals, Which Are Labeled As Samples 1−5 According to the Composition Parameter x

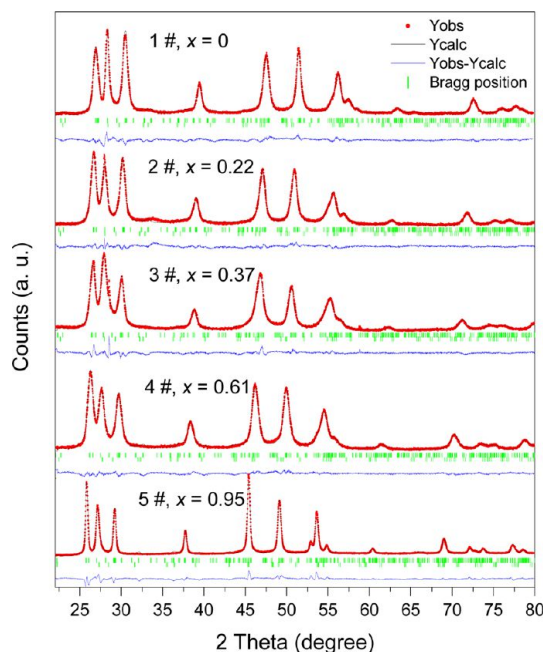| sample	Cu:Zn:Sn	composition x of $Cu_2ZnSn(S_{1-x}Se_x)_4$
1	2:1.2:1.1	0
2	2:1.2:0.9	0.22
3	2:1.1:1.1	0.37
4	2:1.1:1	0.61
5	2:1.1:1	0.95

Figure 4. PXRD patterns and the Rietveld fits of samples 1−5. The diffraction peaks of the obtained wurtzite-derived CZTSSe nanocrystals systemically shift to smaller angles as composition x decreases. Due to the coexistence of zincblende-derived structure, the relative intensities of those shared peaks are slightly intensified.

dispersibility, but the decomposition of 1-dodecanethiol at 280 °C makes the obtained nanocrystals sulfur-doped. In order to get dispersible nanocrsytals with a composition close to pure CZTSe, we added excess diphenyl diselenide to depress the reactivity of 1-dodecanethiol.

The average chemical compositions of the target nanocrystals were studied by the energy dispersive spectrum (EDS) analysis (Figure S2 and Table 2), where we confirmed that the cation ratios are all close to 2:1:1 and composition parameter x gradually increases from 0 to 0.95. Please note the sulfur contents were calculated based on the EDS-determined Cu, Zn, Sn, and Se contents assuming the nanocrystals are electroneutral and all elements are in the expected oxidation states, because the sulfur signal from the capping agent 1-dodecanethiol obscures the accuracy of the sulfur content determination. For simplicity and clarification,

we label the obtained nanocrystals as samples 1−5 according to the composition parameter x (Table 2).

Figure 4 shows the powder X-ray diffraction (PXRD) patterns of the synthesized CZTSSe nanocrystals, together with the Rietveld fits for analyzing the phase purities. Note that the calculated miscibility temperature (200 K) of the wurtzite-derived CZTSSe alloy is much lower than the growth temperature of nanocrystals here (553 K), and it is reasonable to expect that the anion sublattice is occupied by the mixed S and Se anions. Furthermore, wurtzite−kesterite and kesterite are the ground states of the wurtzite- and zincblende-derived CZTS (or CZTSe), respectively, so Rietveld refinements here were performed based on these two structure models with randomly occupied (S+Se) anion sublattices. We found that the phase purities of wurtzite-derived structures in samples 1, 2, 4, and 5 are all high (around 90%) while there is more zincblende phase in sample 3 (32.48%) (Table S4); the byproducts of all samples are zincblende-derived CZTSSe. Even though the experimental data fit well with the simulated data based on the cation-ordered structure models, (Cu+Zn) disorder or partial disorder cannot be detected by only PXRD analysis, and they are possibly present in all synthesized nanocrystals due to the low disorder formation enthalpy.[37,46,48,49] The peak positions systematically shift to smaller angles as the composition parameter x increases, and accordingly, the calculated lattice parameters of samples 1−5 shift gradually to larger values (Table S4 and Figure S3), confirming the obtained nanocrsytals are mixed-anion alloys rather than the phase-segregated mixtures of CZTS and CZTSe.

Since wurtzite ZnS (PCPDF 89-2942) (ZnSe, PCPDF 89-2940) and wurtzite-derived Cu_3SnS_4 (Cu_2SnSe_3)[24,50] show similar PXRD patterns to the wurtzite-derived CZTSSe alloys, additional room-temperature Raman spectra analysis was performed to confirm the obtained nanocrystals are not mixtures of ZnS (ZnSe) and wurtzite-derived Cu_3SnS_4 (Cu_2SnSe_3). Although there are no existing Raman spectra of wurtzite-derived CZTS and CZTSe, they can be expected to show similar Raman spectra to zincblende-derived CZTS and CZTSe, like zincblende ZnS shows similar Raman spectrum to wurtzite ZnS.[51] Zincblende-derived CZTS and CZTSe represent the most intense peaks located at 196 and 338 cm^{-1}, respectively,[29,30] which almost match the most intense peaks of sample 1 and sample 5 (Figure 5), respectively, where the red shift of peaks can be understood by the defect and size effects.[52−54] Wurtzite ZnSe shows the most intense Raman peak at 253 cm^{-1},[51,55] which is not noticeable in the Raman spectrum of sample 5. Wurtzite ZnS has the strongest Raman peak at 351 cm^{-1} located between the most intense peak and another weak peak of CZTS.[13] Even broadening of two neighboring peaks makes the strongest peak of wurtzite ZnS hard to distinguish;
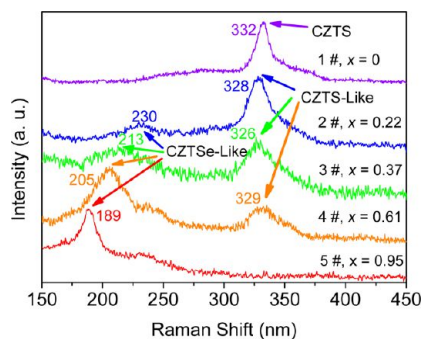

Figure 5. Room-temperature Raman spectra of samples 1−5. The spectra of samples 1 and 5 almost match with those of pure CZTS and CZTSe, respectively; the two typical modes of samples 2−4, i.e., one CZTS-like and the other CZTSe-like mode, generally shifting to smaller wave numbers with increasing composition x, are similar to the observations in the zincblende-derived CZTSSe thin-film samples.
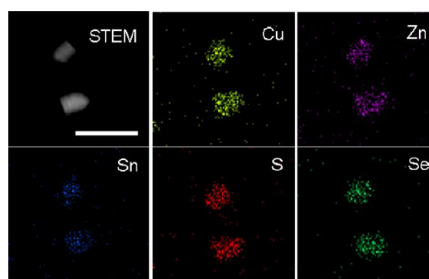

Figure 6. STEM−EDS element mapping of sample 4 with $x = 0.61$, which is the most representative sample among the five samples because it shows the largest formation enthalpy. The five elements present a homogeneous distribution of the characterized nanocrystals, and thus the element distributions of the other four samples can be expected to be homogeneous. The white scale bar in the STEM image is 50 nm.

it is obvious that there is no or very little ZnS in sample 1. Therefore, we can confirm that samples 1 and 5 are not mixtures of binary and ternary chalcogenides with coincidental amounts. With regard to samples 2−4, the strongest Raman peaks represent typical two-mode behaviors (one CZTS-like mode and one CZTSe mode), and generally, both modes shift to higher frequencies with the increment in the content of lighter sulfur atoms (Figure 5). This is consistent with the observations in the Raman spectra of zincblende-derived CZTSSe alloys.[30]

High-resolution scanning transmission electron microscopy (STEM)−EDS element mapping was used to directly observe the element distribution in the wurtzite-derived CZTSSe nanocrystals. According to the theoretical calculations (Figure 2), wurtzite-derived CZTSSe alloys show the largest formation enthalpy with $x = 0.5$; that is to say, the phase segregation will most probably happen in sample 4 with a composition parameter $x = 0.61$, and thus the element distribution in sample 4 is rather representative. It can be seen from Figure 6 that five elements distribute homogeneously among the nanocrsytals and the phase segregation is absent in the nanocrsytals. For samples 1, 2, 3, and 5
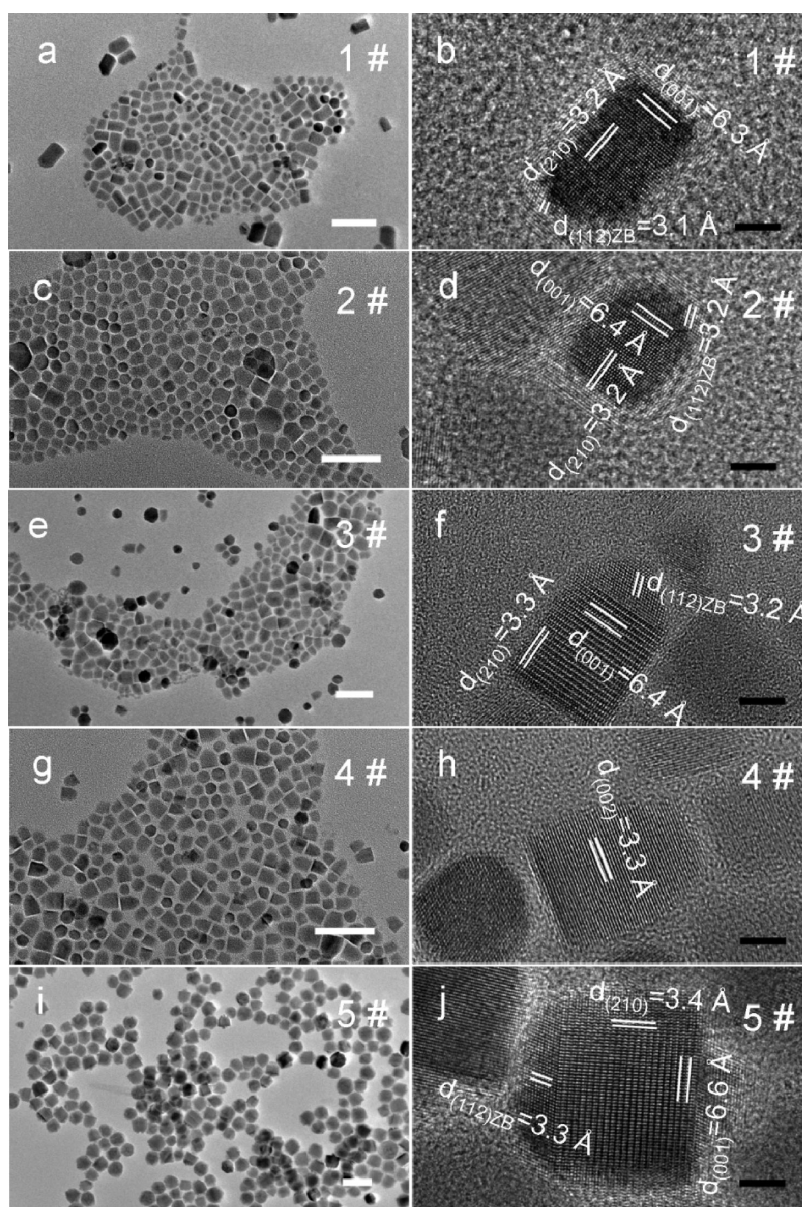
Figure 7. TEM and HRTEM images of samples 1−5. The dimensions of samples 1−5 fall in the ranges 18 ± 10, 20 ± 10, 18 ± 7, 17 ± 5, and 26 ± 4 nm, respectively. The epitaxially grown zincblende-derived CZTSSe can be directly observed in the HRTEM images. The white and black scale bars are 50 and 5 nm, respectively.

with lower anion mixing enthalpies, it is reasonable to confirm that they also do not encounter the problem of phase segregation.

The transmission electron microscopy (TEM) images in Figure 7 show the sizes and morphologies of the obtained CZTSSe nanocrystals. The dimensions of samples 1−5 fall in the ranges 18 ± 10, 20 ± 10, 18 ± 7, 17 ± 5, and 26 ± 4 nm, respectively. We calculated the exciton Bohr radius a_B of CZTS and CZTSe using the reported values[56] following the equation

$$a_B = \frac{\hbar^2 \varepsilon}{e^2}\left(\frac{1}{m_e} + \frac{1}{m_h}\right)$$

$$= 0.053 \varepsilon m_o \left(\frac{1}{m_e} + \frac{1}{m_h}\right) \text{ (nm)} \qquad (3)$$

where $\hbar$, ε, m_e, m_h, and m_o are the reduced plank constant, dielectric constant, effective mass of electron, effective mass of hole, and rest mass of electron, respectively.[57] The calculated a_B of CZTS and CZTSe are 2.2−4.3 and 6.38−13.25 nm, respectively. CZTSe has a much larger exciton Bohr radius than CZTS, but they are still smaller than the average dimensions of the nanocrsytals among all five samples, indicating that quantum confinement does not have an effective impact on the band gaps of the synthesized nanocrsytals. HRTEM images reveal that the major phases of the CZTSSe nanocrsytals are wurtzite-derived structures, and there are also several or tens of anion atom layers stacked with the sequence ...ABCABC..., which is the typical sequence of a zincblende-derived structure,
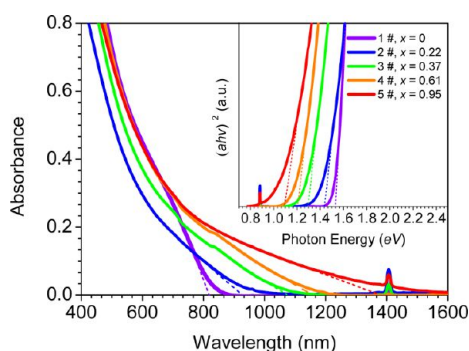
Figure 8. UV−vis−NIR spectra of samples 1−5, which are stably dispersed in hexane. The linearly extrapolated onsets of the samples decrease with increasing composition *x*. The inset is the linear extrapolation of $(\alpha h\nu)^2$ *versus* photon energy, from which the band gaps evaluated also decrease as composition *x* increases. The absorbance peaks in the UV−vis−NIR spectra located around 1400 nm are attributed to hexane.
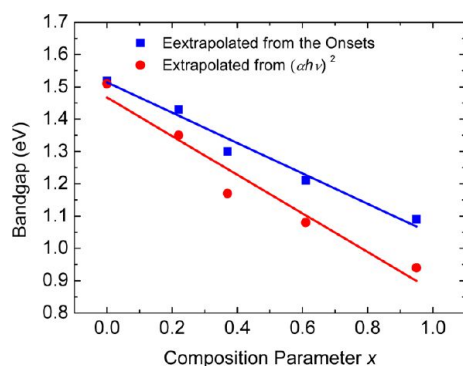

Figure 9. Experimental band gaps of samples 1−5, which decrease almost linearly from 1.5 eV to about 1 eV with increasing composition parameter *x* from 0 to 0.95.

interfacing with the wurtzite-derived domains along the $[001]_{WZ}$ direction. The results here are consistent with those obtained from the Rietveld refinement analysis. It has been found that the band gap of wurtzite GaAs nanowires slightly downshifts with the presence of zincblende segments,[58] so the small amount of co-existing zincblende-derived CZTSSe structures can affect the band gaps of wurtzite-derived CZTSSe structures to some extent.[59] However, when we compare the band gaps of CZTSSe nanocrystals with different composition *x*, the effect of a coexisting zincblende-derived structure should be small, because zincblende-derived structures are only minority phases existing in all samples.

Experimental Band-Gap Dependence on Composition of the Wurtzite-Derived CZTSSe Alloy Nanocrystals. Figure 8 illustrates the UV−vis−NIR spectra of a CZTSSe alloy nanocrystal stably dispersed in hexane. Before the measurements, the absorbances of different samples were tuned to be close to each other through adjusting the concentrations of the colloidal dispersions. We calculated the light absorption coefficient α from the equation α = A/bc, where the A, b, and c are the absorbance, cuvette thickness (1 cm), and nanocrystal

concentration (defined as 1). Please note that the calculated absorption coefficient here is used only for estimating the band gaps but not for evaluating the light absorbance capacities of the nanocrsytals. The band gaps of the CZTSSe alloy nanocrsytals were evaluated by two widely used methods for direct bandgap semiconductors, *i.e.*, linear extrapolation of the absorbance onset *versus* wavelength and $(\alpha h\nu)^2$ *versus* photon energy. It can be clearly observed from Figure 9 that the band gaps of CZTSSe alloy nanocrystals almost linearly decrease with increasing composition *x*, regardless of the estimating method. We noticed the variations in cation ratios of five samples (Table 1), and actually, Zn doping will enlarge the band gaps of CZTS and CZTSe, while Sn doping will decrease the band gaps. Samples 1 and 2 show the same Cu/Zn ratio, while the Sn content in sample 2 is about 20% lower than sample 1; however, the band gap of sample 2 is smaller than that of sample 1, indicating the S/Se ratio plays a dominant role in the band-gap determination. Sample 3 has a lower Zn content, and together with a higher Sn content than sample 2, this might be the reason that the band gap of sample 3 is a little bit lower than the lineally fitted value. In general, all five samples vary slightly in cation ratios, but the band gaps almost decrease linearly with decreasing S/Se ratio, indicating the band gaps of CZTSSe nanocrystals are mainly effected by S/Se ratios.

For wurtzite-derived CZTS and CZTSSe alloy nanocrystals with *x* = 0.95, the measured band gaps are about 1.5 and 1 eV, respectively, showing a tunable range of 0.5 eV. Tunable ranges of 0.22 (1.28−1.50[28]) and 0.07 eV (1.47−1.54 eV[20]) have been achieved previously through tuning the compositions of zincblende-derived CZTSSe alloy nanocrystals.[20,28] In contrast, our experimental result reveals that a much larger tunable range can be obtained in wurtzite-derived CZTSSe alloy nanocrystals. Both the band-gap range and bowing from the experimental measurements show good agreement with the theoretically calculated values.

CONCLUSIONS

To conclude, we performed a combined theoretical and experimental study on wurtzite-derived CZTSSe alloys. The calculations predict that the wurtzite-derived CZTS and CZTSe are miscible above 200 K and the band gaps of CZTSSe alloys can be linearly tuned from 1.0 to 1.5 eV through adjusting the composition parameter *x*. We prepared CZTSSe alloy nanocrystals with composition parameter *x* varying from 0 to 0.95 and evaluated their band gaps from the UV−vis−NIR spectra. The experimental results confirm the theoretical prediction that the band gaps of wurtzite-derived CZTSSe alloy nanocrystals increase almost linearly from about 1.0 to 1.5 as *x* increases from 0 to 0.95, and the tunable range (0.5 eV) is much larger than the previously

reported values (0.07 and 0.22 eV)[20,28] for zincblende-derived samples. To the best of our knowledge, this is the first investigation of wurtzite-derived CZTSSe alloys in either theory or experiment.

METHODS

Calculation Methods. The total energy and electronic band structure have been calculated within the density functional formalism as implemented in the VASP code.[20,27,60] For the exchange–correlation potential, we used the generalized gradient approximation (GGA) of Perdew and Wang, known as PW91.[61] The d states of group IV elements are treated explicitly as valence. The interaction between the core electrons and the valence electrons is included by the standard frozen-core projector augmented wave potentials. An energy cutoff of 300 eV was applied in all cases. For Brillouin-zone integration, we used k-point meshes that are equivalent to the $6 \times 6 \times 6$ Monkhorst–Pack meshes for a 16-atom orthorhombic unit cell. All lattice vectors and atomic positions were fully relaxed by minimizing the quantum mechanical stresses and forces.

Chemicals. Hexane (97%), ethanol (99.7%), 1-dodecanethiol (97%), CuI (99.5%), Zn(CH$_3$COO)$_2\cdot$2H$_2$O (99%), and SnCl$_2\cdot$2H$_2$O (98%) were purchased from Sinopharm Chemical Reagent Co. Ltd. (Shanghai). Oleylamine (80–90%) was purchased from Aladdin Reagent Co. Ltd. (Shanghai). Diphenyl diselenide (99%) was purchased from Acros Organics. All chemical reagents were used as received without further purification.

Synthesis of Wurtzite-Derived CZTSSe Nanocrystals with Different Composition x. To prepare wurtzite-derived CZTSSe nanocrsytals with tunable composition x, different amounts of CuI, Zn-(CH$_3$COO)$_2\cdot$2H$_2$O, and SnCl$_2\cdot$2H$_2$O listed in Table S3 were dissolved in 10 mL of oleylamine in the presence of various amounts of 1-dodecanethiol (Table S3) in a three-neck flask in air and then heated to 180 °C. At the same time, various amounts of diphenyl diselenide, which are also listed in Table S1, were dissolved in another three-neck flask containing 5 mL of oleylamine in air at 70 °C. Reactions were started through injecting diphenyl diselenide solution into the former salt solution. (For the synthesis of pure CZTS nanocrsytals, these two steps have not been performed.) The reaction temperature was increased from 150 °C to 280 °C at a heating rate of 10 °C/min and kept at 280 °C for 0.5 h.

When the reactions were completed, the reaction flasks were removed from the heating mantles and naturally cooled. The black products were collected and centrifuged at 8000 rpm for 5 min, and the upper clear yellow solutions were discarded. Then hexane was added to disperse the nanocrystals. The dispersions were centrifuged at 4000 rpm for 5 s; larger nanocrystals and aggregates were discarded, while the bright black colloidal solutions were transferred into another centrifuge tube, where slurries formed after the addition of ethanol. Those slurries were centrifuged again at 8000 rpm for 5 min, and the nanocrystals were accumulated at the bottom of centrifuge tube once again. The washing process was repeated two times. A typical reaction yields about 20 mg of dispersible nanocrystals.

Measurement and Characterization. The crystalline structure of the products was characterized by PXRD, using a Philips X'Pert PRO SUPER X-ray diffractometer equipped with graphite-monochromated Cu Kα radiation (λ = 1.54056 Å). The operation voltage and current were kept at 40 kV and 400 mA, respectively. The phase purities and relationships were analyzed using the X'pert High Score Plus software in conjunction with the ICDD database. All structural refinements were carried out using the Rietveld refinement technique with the Fullprof software suite (version 2.05).[62] For zincblende- and wurtzite-derived CZTSSe, the space groups were taken as $I\bar{4}$ and P1. Pseudo-Voigt profile functions were employed, and 18 least-squares parameters (zero-point parameter, scale factor, lattice parameters, profile parameters U, V, W, shape, X, Asy) were varied during the refinement process.

Nanocrystals dispersed in hexane were drop-casted on carbon-supported Mo grids for TEM and HRTEM observations, which were performed on JEOL-2010F with an acceleration voltage of 200 kV. EDS and STEM-EDS element mapping were carried out on an Inca Oxford equipped on a JEOL-2010F, and Be grids were used for STEM-EDS mapping (*Please note that Be grids are highly toxic and should be handled with extreme caution*).

Conflict of Interest: The authors declare no competing financial interest.

Supporting Information Available: Detailed information about the wurtzite–kesterite and kesterite CZTSSe, SQS model of wurtzite-derived CZTSSe with different compositions x, the amounts of cation and anion sources used for reactions, EDS spectra of the synthesized nanocrsytals, parameters of the Rietveld fits and refined lattice parameters, and phase purities. This material is available free of charge *via* the Internet at http://pubs.acs.org.

REFERENCES AND NOTES

1. Seol, J. S.; Lee, S. Y.; Lee, J. C.; Nam, H. D.; Kim, K. H. Electrical and Optical Properties of Cu$_2$ZnSnS$_4$ Thin Films Prepared by RF Magnetron Sputtering Process. *Sol. Energy Mater. Sol. Cells* **2003**, *75*, 155–162.
2. Katagiri, H. Cu$_2$ZnSnS$_4$ Thin Film Solar Cells. *Thin Solid Films* **2005**, *480*, 426–432.
3. Kim, K. H.; Wibowo, R. A.; Kim, W. S.; Lee, E. S.; Munir, B. Single Step Preparation of Quaternary Cu$_2$ZnSnSe$_4$ Thin Films by RF Magnetron Sputtering from Binary Chalcogenide Targets. *J. Phys. Chem. Solids* **2007**, *68*, 1908–1913.
4. Todorov, T. K.; Reuter, K. B.; Mitzi, D. B. High-Efficiency Solar Cell with Earth-Abundant Liquid-Processed Absorber. *Adv. Mater.* **2010**, *22*, E156–E159.
5. Barkhouse, D. A. R.; Gunawan, O.; Gokmen, T.; Todorov, T. K.; Mitzi, D. B. Device Characteristics of a 10.1% Hydrazine-Processed Cu$_2$ZnSn(Se,S)$_4$ Solar Cell. *Prog. Photovoltaics* **2012**, *20*, 6–11.
6. Gur, I.; Fromer, N. A.; Geier, M. L.; Alivisatos, A. P. Air-Stable All-Inorganic Nanocrystal Solar Cells Processed from Solution. *Science* **2005**, *310*, 462–465.
7. Guo, Q.; Kim, S. J.; Kar, M.; Shafarman, W. N.; Birkmire, R. W.; Stach, E. A.; Agrawal, R.; Hillhouse, H. W. Development of CuInSe$_2$ Nanocrystal and Nanoring Inks for Low-Cost Solar Cells. *Nano Lett.* **2008**, *8*, 2982–2987.
8. Panthani, M. G.; Akhavan, V.; Goodfellow, B.; Schmidtke, J. P.; Dunn, L.; Dodabalapur, A.; Barbara, P. F.; Korgel, B. A. Synthesis of CuInS$_2$, CuInSe$_2$, and Cu(In$_x$Ga$_{1-x}$)Se$_2$ (CIGS) Nanocrystal "Inks" for Printable Photovoltaics. *J. Am. Chem. Soc.* **2008**, *130*, 16770–16777.
9. Nozik, A. J.; Luther, J. M.; Law, M.; Beard, M. C.; Song, Q.; Reese, M. O.; Ellingson, R. J. Schottky Solar Cells Based on Colloidal Nanocrystal Films. *Nano Lett.* **2008**, *8*, 3488–3492.
10. Guo, Q.; Ford, G. M.; Hillhouse, H. W.; Agrawal, R. Sulfide Nanocrystal Inks for Dense Cu(In$_{1-x}$Ga$_x$)(S$_{1-y}$Se$_y$)$_2$ Absorber Films and Their Photovoltaic Performance. *Nano Lett.* **2009**, *9*, 3060–3065.

11. Guo, Q.; Hillhouse, H. W.; Agrawal, R. Synthesis of Cu_2ZnSnS_4 Nanocrystal Ink and Its Use for Solar Cells. *J. Am. Chem. Soc.* **2009**, *131*, 11672–11673.

12. Riha, S. C.; Parkinson, B. A.; Prieto, A. L. Solution-Based Synthesis and Characterization of Cu_2ZnSnS_4 Nanocrystals. *J. Am. Chem. Soc.* **2009**, *131*, 12054–12055.

13. Steinhagen, C.; Panthani, M. G.; Akhavan, V.; Goodfellow, B.; Koo, B.; Korgel, B. A. Synthesis of Cu_2ZnSnS_4 Nanocrystals for Use in Low-Cost Photovoltaics. *J. Am. Chem. Soc.* **2009**, *131*, 12554–12555.

14. Guo, Q.; Ford, G. M.; Yang, W. C.; Walker, B. C.; Stach, E. A.; Hillhouse, H. W.; Agrawal, R. Fabrication of 7.2% Efficient CZTSSe Solar Cells Using CZTS Nanocrystals. *J. Am. Chem. Soc.* **2010**, *132*, 17384–17386.

15. Guo, Q.; Ford, G. M.; Agrawal, R.; Hillhouse, H. W. Ink Formulation and Low-Temperature Incorporation of Sodium to Yield 12% Efficient Cu(In,Ga)(S,Se)$_2$ Solar Cells from Sulfide Nanocrystal Inks. *Prog. Photovoltaics* **2013**, *21*, 64–71.

16. Guo, Q.; Ford, G. M.; Yang, W. C.; Hages, C. J.; Hillhouse, H. W.; Agrawal, R. Enhancing the Performance of CZTSSe Solar Cells with Ge Alloying. *Sol. Energy Mater. Sol. Cells* **2012**, *105*, 132–136.

17. Shi, L.; Pei, C.; Xu, Y.; Li, Q. Template-Directed Synthesis of Ordered Single-Crystalline Nanowires Arrays of Cu_2ZnSnS_4 and $Cu_2ZnSnSe_4$. *J. Am. Chem. Soc.* **2011**, *133*, 10328–10331.

18. Singh, A.; Geaney, H.; Lafir, F.; Ryan, K. M. Colloidal Synthesis of Wurtzite Cu_2ZnSnS_4 Nanorods and Their Perpendicular Assembly. *J. Am. Chem. Soc.* **2012**, *134*, 2910–3913.

19. Wang, J. J.; Xue, D. J.; Guo, Y. G.; Hu, J. S.; Wan, L. J. Bandgap Engineering of Monodispersed $Cu_{2-x}S_ySe_{1-y}$ Nanocrystals through Chalcogen Ratio and Crystal Structure. *J. Am. Chem. Soc.* **2011**, *133*, 18558–18561.

20. Riha, S. C.; Parkinson, B. A.; Prieto, A. L. Compositionally Tunable $Cu_2ZnSn(S_{1-x}Se_x)_4$ Nanocrystals: Probing the Effect of Se-Inclusion in Mixed Chalcogenide Thin Films. *J. Am. Chem. Soc.* **2011**, *133*, 15272–15275.

21. Regulacio, M. D.; Ye, C.; Lim, S. H.; Bosman, M.; Ye, E.; Chen, S.; Xu, Q. H.; Han, M. Y. Colloidal Nanocrystals of Wurtzite-Type Cu_2ZnSnS_4: Facile Noninjection Synthesis and Formation Mechanism. *Chem.—Eur. J.* **2012**, *18*, 3127–3131.

22. Pan, D. C.; An, L. J.; Sun, Z. M.; Hou, W.; Yang, Y.; Yang, Z. Z.; Lu, Y. F. Synthesis of Cu-In-S Ternary Nanocrystals with Tunable Structure and Composition. *J. Am. Chem. Soc.* **2008**, *130*, 5620–5621.

23. Norako, M. E.; Brutchey, R. L. Synthesis of Metastable Wurtzite $CuInSe_2$ Nanocrystals. *Chem. Mater.* **2010**, *22*, 1613–1615.

24. Norako, M. E.; Greaney, M. J.; Brutchey, R. L. Synthesis and Characterization of Wurtzite-Phase Copper Tin Selenide Nanocrystals. *J. Am. Chem. Soc.* **2012**, *134*, 23–26.

25. Lu, X. T.; Zhuang, Z. B.; Peng, Q.; Li, Y. D. Wurtzite Cu_2ZnSnS_4 Nanocrystals: A Novel Quaternary Semiconductor. *Chem. Commun.* **2011**, *47*, 3141–3143.

26. Wang, J. J.; Hu, J. S.; Guo, Y. G.; Wan, L. J. Wurtzite $Cu_2ZnSnSe_4$ Nanocrystals for High-Performance Organic−Inorganic Hybrid Photodetectors. *NPG Asia Mater.* **2012**, *4*, e2.

27. Chen, S. Y.; Walsh, A.; Yang, J. H.; Gong, X. G.; Sun, L.; Yang, P. X.; Chu, J. H.; Wei, S. H. Compositional Dependence of Structural and Electronic Properties of $Cu_2Znsn(S,Se)_4$ Alloys for Thin Film Solar Cells. *Phys. Rev. B* **2011**, 83.

28. Yang, Z.; Wei, H.; Ye, Z. C.; Li, M.; Su, Y. J.; Zhang, Y. F. Tunable Band Gap $Cu_2ZnSnS_{4x}Se_{4(1-x)}$ Nanocrystals: Experimental and First-Principles Calculations. *CrystEngComm* **2011**, *13*, 2222–2226.

29. Grossberg, M.; Krustok, J.; Raudoja, J.; Timmo, K.; Altosaar, M.; Raadik, T. Photoluminescence and Raman Study of $Cu_2ZnSn(Se_xS_{1-x})_4$ Monograins for Photovoltaic Applications. *Thin Solid Films* **2011**, *519*, 7403–7406.

30. He, J.; Sun, L.; Chen, S. Y.; Chen, Y.; Yang, P. X.; Chu, J. H. Composition Dependence of Structure and Optical Properties of $Cu_2ZnSn(S,Se)_4$ Solid Solutions: An Experimental Study. *J. Alloys Compd.* **2012**, *511*, 129–132.

31. Chiang, M. Y.; Chang, S. H.; Chen, C. Y.; Yuan, F. W.; Tuan, H. Y. Quaternary $CuIn(S_{1-x}Se_x)_2$ Nanocrystals: Facile Heating-up Synthesis, Band Gap Tuning, and Gram-Scale Production. *J. Phys. Chem. C* **2011**, *115*, 1592–1599.

32. Wang, G. J.; Cheng, G.; Hu, B. B.; Wang, X. L.; Wan, S. M.; Wu, S. X.; Du, Z. L. Preparation of $CuIn(S_xSe_{1-x})_2$ Thin Films with Tunable Band Gap by Controlling Sulfurization Temperature of $CuInSe_2$. *J. Mater. Res.* **2010**, *25*, 2426–2429.

33. Caetano, C.; Teles, L. K.; Marques, M.; Dal Pino, A., Jr.; Ferreira, L. G. Phase Stability, Chemical Bonds, and Gap Bowing of $In_xGa_{1-x}N$ Alloys: Comparison between Cubic and Wurtzite Structures. *Phys. Rev. B* **2006**, *74*, 045215.

34. Levander, A. X.; Liliental-Weber, Z.; Broesler, R.; Hawkridge, M. E.; Novikov, S. V.; Foxon, C. T.; Dubon, O. D.; Wu, J.; Walukiewicz, W.; Yu, K. M. Thermal Stability of Amorphous $GaN_{1-x}As_x$ Alloys. *Appl. Phys. Lett.* **2011**, *98*, 161902.

35. Locmelis, S.; Brunig, C.; Binnewies, M.; Borger, A.; Becker, K. D.; Homann, T.; Bredow, T. Optical Band Gap in the System $ZnO_{1-x}S_x$. An Experimental and Quantum Chemical Study. *J. Mater. Sci.* **2007**, *42*, 1965–1971.

36. Chen, S. Y.; Gong, X. G.; Walsh, A.; Wei, S. H. Electronic Structure and Stability of Quaternary Chalcogenide Semiconductors Derived from Cation Cross-Substitution of II-VI and I-III-VI$_2$ Compounds. *Phys. Rev. B* **2009**, *79*, 165211.

37. Chen, S. Y.; Walsh, A.; Luo, Y.; Yang, J. H.; Gong, X. G.; Wei, S. H. Wurtzite-Derived Polytypes of Kesterite and Stannite Quaternary Chalcogenide Semiconductors. *Phys. Rev. B* **2010**, *82*, 195203.

38. Kim, K. J.; Lee, M. H.; Bahng, J. H.; Shim, K.; Choe, B. D. Optical Constants and Electronic Interband Transitions of Disordered $GaAs_{1-x}P_x$ Alloys. *J. Appl. Phys.* **1998**, *84*, 3696–3699.

39. Wei, S. H.; Ferreira, L. G.; Bernard, J. E.; Zunger, A. Electronic-Properties of Random Alloys - Special Quasirandom Structures. *Phys. Rev. B* **1990**, *42*, 9622–9649.

40. Zunger, A.; Wei, S. H.; Ferreira, L. G.; Bernard, J. E. Special Quasirandom Structures. *Phys. Rev. Lett.* **1990**, *65*, 353–356.

41. Wei, S. H.; Zunger, A. Band Offsets and Optical Bowings of Chalcopyrites and Zn-Based II-VI Alloys. *J. Appl. Phys.* **1995**, *78*, 3846–3856.

42. Ludwig, C. D. R.; Gruhn, T.; Felser, C.; Schilling, T.; Windeln, J.; Kratzer, P. Indium-Gallium Segregation in $CuIn_xGa_{1-x}Se_2$: An Ab Initio-Based Monte Carlo Study. *Phys. Rev. Lett.* **2010**, *105*, 025702.

43. Shavel, A.; Arbiol, J.; Cabot, A. Synthesis of Quaternary Chalcogenide Nanocrystals: Stannite $Cu_2Zn_xSn_ySe_{1+x+2y}$. *J. Am. Chem. Soc.* **2010**, *132*, 4514–4515.

44. Wei, H.; Guo, W.; Sun, Y. J.; Yang, Z.; Zhang, Y. F. Hot-Injection Synthesis and Characterization of Quaternary $Cu_2ZnSnSe_4$ Nanocrystals. *Mater. Lett.* **2010**, *64*, 1424–1426.

45. Ahn, S.; Jung, S.; Gwak, J.; Cho, A.; Shin, K.; Yoon, K.; Park, D.; Cheong, H.; Yun, J. H. Determination of Band Gap Energy (E_g) of $Cu_2ZnSnSe_4$ Thin Films: On the Discrepancies of Reported Band Gap Values. *Appl. Phys. Lett.* **2010**, *97*, 021905.

46. Chen, S. Y.; Gong, X. G.; Walsh, A.; Wei, S. H. Crystal and Electronic Band Structure of Cu_2ZnSnX_4 (X=S and Se) Photovoltaic Absorbers: First-Principles Insights. *Appl. Phys. Lett.* **2009**, *94*, 041903.

47. Fan, F.-J.; Wang, Y.-X.; Liu, X.-J.; Wu, L.; Yu, S.-H. Large-Scale Colloidal Synthesis of Non-Stoichiometric $Cu_2ZnSnSe_4$ Nanocrystals for Thermoelectric Applications. *Adv. Mater.* **2012**, *24*, 6158–6163.

48. Schorr, S. The Crystal Structure of Kesterite Type Compounds: A Neutron and X-Ray Diffraction Study. *Sol. Energy Mater. Sol. Cells* **2011**, *95*, 1482–1488.

49. Schorr, S.; Hoebler, H. J.; Tovar, M. A Neutron Diffraction Study of the Stannite-Kesterite Solid Solution Series. *Eur. J. Mineral* **2007**, *19*, 65–73.

50. Yi, L.; Wang, D.; Gao, M. Synthesis of Cu_3SnS_4 Nanocrystals and Nanosheets by Using $Cu_{31}S_{16}$ as Seeds. *CrystEngComm* **2012**, *14*, 401–404.

51. Cheng, Y. C.; Jin, C. Q.; Gao, F.; Wu, X. L.; Zhong, W.; Li, S. H.; Chu, P. K. Raman Scattering Study of Zinc Blende and Wurtzite ZnS. *J. Appl. Phys.* **2009**, *106*, 123505.

52. Zeiri, L.; Patla, I.; Acharya, S.; Golan, Y.; Efrima, S. Raman Spectroscopy of Ultranarrow CdS Nanostructures. *J. Phys. Chem. C* **2007**, *111*, 11843–11848.

ARTICLE

53. Yang, C. C.; Li, S. Size-Dependent Raman Red Shifts of Semiconductor Nanocrystals. *J. Phys. Chem. B* **2008**, *112*, 14193–14197.

54. Fan, F.-J.; Yu, B.; Wang, Y.-X.; Zhu, Y.-L.; Liu, X.-J.; Yu, S.-H.; Ren, Z.-F. Colloidal Synthesis of $Cu_2CdSnSe_4$ Nanocrytals and Hot-Pressing to Enhance the Thermoelectric Figure-of-Merit. *J. Am. Chem. Soc.* **2011**, *133*, 15910–15913.

55. Shan, C. X.; Liu, Z.; Zhang, X. T.; Wong, C. C.; Hark, S. K. Wurtzite ZnSe Nanowires: Growth, Photoluminescence, and Single-Wire Raman Properties. *Nanotechnology* **2006**, *17*, 5561–5564.

56. Persson, C. Electronic and Optical Properties of Cu_2ZnSnS_4 and $Cu_2ZnSnSe_4$. *J. Appl. Phys.* **2010**, *107*, 053710.

57. Wang, Y.; Herron, N. Nanometer-Sized Semiconductor Clusters - Materials Synthesis, Quantum Size Effects, and Photophysical Properties. *J. Phys. Chem.* **1991**, *95*, 525–532.

58. Heiss, M.; Conesa-Boj, S.; Ren, J.; Tseng, H.-H.; Gali, A.; Rudolph, A.; Uccelli, E.; Peiro, F.; Ramon Morante, J.; Schuh, D.; Reiger, E.; Kaxiras, E.; Arbiol, J.; Fontcuberta i Morral, A. Direct Correlation of Crystal Structure and Optical Properties in Wurtzite/Zinc-Blende GaAs Nanowire Heterostructures. *Phys. Rev. B* **2011**, *83*, 045303.

59. Fan, F.-J.; Wu, L.; Gong, M.; Chen, S. Y.; Liu, G. Y.; Yao, H.-B.; Liang, H.-W.; Wang, Y.-X.; Yu, S.-H. Linearly Arranged Polytypic CZTSSe Nanocrystals. *Sci. Rep.* **2012**, *2*, 952.

60. Kresse, G.; Furthmuller, J. Efficient Iterative Schemes for Ab Initio Total-Energy Calculations Using a Plane-Wave Basis Set. *Phys. Rev. B* **1996**, *54*, 11169–11186.

61. Perdew, J. P.; Chevary, J. A.; Vosko, S. H.; Jackson, K. A.; Pederson, M. R.; Singh, D. J.; Fiolhais, C. Atoms, Molecules, Solids, and Surfaces - Applications of the Generalized Gradient Approximation for Exchange and Correlation. *Phys. Rev. B* **1992**, *46*, 6671–6687.

62. Zalewski, W.; Bacewicz, R.; Antonowicz, J.; Pietnoczka, A.; Evstigneeva, T. L.; Schorr, S. XAFS Study of Kesterite, Kuramite and Stannite Type Alloys. *J. Alloys Compd.* **2010**, *492*, 35–38.